



ELSEVIER

Available online at www.sciencedirect.com

SCIENCE @ DIRECT®

Ocean Modelling 6 (2004) 221–244

Ocean
Modelling

www.elsevier.com/locate/omodel

Conservation of properties in a free-surface model

Jean-Michel Campin ^{*}, Alistair Adcroft, Chris Hill, John Marshall

*Department of Earth, Atmospheric and Planetary Sciences, Massachusetts Institute of Technology,
Cambridge, MA 02139, USA*

Received 27 November 2002; received in revised form 16 January 2003; accepted 16 January 2003

Abstract

In height coordinate ocean models, natural conservation of tracers (temperature, salinity or any passive tracer) requires that the thickness of the surface cell varies with the free-surface displacement, leading to a non-linear free-surface formulation (NLFS). However, NLFS does not guarantee exact conservation unless special care is taken in the implementation, and in particular the time stepping scheme, as pointed out by Griffies et al. (*Monthly Weather Rev.* 129 (2001) 1081).

This paper presents a general method to implement a NLFS in a conservative way, using an implicit free surface formulation. Details are provided for two tracer time stepping schemes, both second order in time and space: a two time-level scheme, such as Lax–Wendroff scheme, guarantees exact tracer conservation; a three time-level scheme such as the Adams–Bashforth II requires further adaptations to achieve exact local conservation and accurate global conservation preventing long term drift of the model tracer content. No compromise is required between local and global conservation since the method accurately conserves any tracer. In addition to the commonly used backward time stepping, the implicit free surface formulation also offers the option of a Crank–Nickelson time stepping which conserves the energy.

The methods are tested in idealized experiments designed to emphasize problems of tracer and energy conservation. The tests show the ability of the NLFS method to conserve tracers, in contrast to the linear free-surface formulation. A test of energy conservation reveals that free-surface backward time-stepping strongly damps the solution. In contrast, Crank–Nickelson time stepping exactly conserves energy in the pure linear case and confirms the NLFS improvement relative to the linear free-surface when momentum advection is included.

© 2003 Elsevier Ltd. All rights reserved.

Keywords: Free-surface; Tracer conservation; Shallow water equations; General circulation models

^{*} Corresponding author.

E-mail addresses: jmc@ocean.mit.edu (J.-M. Campin), adcroft@mit.edu (A. Adcroft), cnh@plume.mit.edu (C. Hill), marshall@gulf.mit.edu (J. Marshall).

1. Introduction

Ocean general circulation models built in height coordinates have almost universally adopted a free-surface formulation over the rigid-lid method (see e.g., Killworth et al., 1991; Dukowicz and Smith, 1994; Griffies et al., 2000). This is because a free surface is dynamically more accurate but also because the free-surface equations prove to be more efficient than solving the costly elliptic equation required when using a rigid-lid.

There are various ways of solving the free-surface equations. These derive from two basic assumptions: (i) there is a separation of time-scales between the external gravity mode and internal dynamics and (ii) displacements in free-surface height are small compared to the depth of the open ocean. The first assumption leads to two numerical approaches (a) the split-explicit free-surface (Killworth et al., 1991) and (b) the semi-implicit free-surface (Dukowicz and Smith, 1994; Marshall et al., 1997a). The second assumption, of small height deviations, justifies a linearization of the free-surface height equation simplifying the solution procedure and, in particular, rendering the implicit approach easier to implement. Whatever approach is used, conservation properties of the model are intimately linked to the treatment of the free-surface. Without special treatment, local and global conservation of tracers are not guaranteed. For example, using a linearized free-surface and a flux-form representation of tracer advection, a “surface correction” term is required at the surface to maintain local conservation but cannot guarantee global conservation (Griffies et al., 2000).

Use of the unapproximated (non-linear) free-surface equation is more accurate. Griffies et al. (2001) outlined an approach using the leap-frog time-stepping for tracers and momentum and a split-explicit time-stepping of the unapproximated (non-linear) free-surface equation. They distinguish between two conservation issues: (1) Globally, the evolution of the volume integrated tracer content must equal the integrated surface flux. In the special case that the surface flux of tracer is identically zero, this global constraint implies constant global tracer content. (2) Locally, tracer and free-surface discretization must be compatible with one another to ensure that a homogeneous tracer remains unaffected by free-surface undulations. Griffies et al. (2001) point out that in the presence of time filtering (required for the stability of Leap-frog time stepping scheme), local and global tracer conservation cannot simultaneously be achieved. In the presence of filtering of the tracer *concentration* only local conservation of tracers can be achieved. In contrast, when a time filter is applied to tracer *content* (i.e. the product of the level thickness and tracer concentration), global conservation is satisfied but not local. Although the drift in total tracer content is generally small (Griffies et al., 2001), this detracts from the advantage of the non-linear free surface formulation since its dynamical effects are also relatively small (Roullet and Madec, 2000).

The purpose of this paper is to build on the study of Griffies et al. (2001) to derive free surface schemes that have both local and global conservation. A non-linear free surface formulation (NLFS) has been implemented within the MITgcm model (Marshall et al., 1997a), and is shown to exactly conserve any tracer, both locally and globally. The original implicit surface pressure method has been modified rather than replaced by the split-explicit method. Contrary to what has been previously suggested (Griffies et al., 2000), the implicit method can perfectly be used without any approximation relatively to the free surface equation. Among several other advantages, the implicit method appears very flexible: it can be used in rigid-lid or free surface mode and is fully

compatible with the non-hydrostatic 3-D pressure solver (Marshall et al., 1997b). In addition, a Crank–Nickelson barotropic time stepping that combines an explicit and implicit part (one half for each) has been implemented with only minor modifications, and provides an unconditionally stable scheme that exactly conserves the total energy, i.e. kinetic energy (KE) plus potential energy (PE) associated with sea surface height (SSH). In contrast, it is difficult to conserve total energy using a split-explicit method because time averaging and/or filtering of barotropic variables is required to stabilize the scheme resulting in damping of total energy¹.

In Section 2 a general method is presented that provides the basis of a conservative implementation of NLFS. The method is similar to that of Griffies et al. (2001) but is formulated in the framework of the implicit free surface method and with a forward two time-level tracer scheme. The method is designed to exactly conserve any tracer, both locally and globally. Assuming a forward two time-level scheme for tracers avoids the difficulties in tracer conservation that Griffies et al. (2001) encounter with leap-frog time stepping and time filtering. We go on to discuss two implementations for two different tracer time stepping schemes: The first one is based on the Lax–Wendroff advection scheme and offers a straightforward illustration of the general method (Section 3). The second is the Adams–Bashforth II, a three time-level scheme (like the leap-frog scheme), that requires further adaptations (Section 4). The methods are tested in two simple configurations in Section 5 confirming the ability of the schemes in Sections 3 and 4, to conserve tracers and energy. The main results are summarized in the conclusions.

2. Time stepping of the free surface equations

For simplicity, we first consider a one layer Boussinesq model. The equations for continuity and tracer concentration T can be written:

$$\partial_t h + \nabla \cdot h\mathbf{v} = P \tag{1}$$

$$\partial_t \mathbf{v} + g\nabla\eta = \mathbf{G}_v \tag{2}$$

$$\partial_t(hT) + \nabla \cdot (hT\mathbf{v}) = PT_{\text{rain}} \tag{3}$$

where $h = H + \eta$ is the height of the water column, H the ocean depth, and η the SSH, \mathbf{v} the velocity vector, g the gravity, P the net precipitation (precipitation plus run-off minus evaporation), and T_{rain} the tracer concentration associated with precipitation P . \mathbf{G}_v contains all momentum contributions (Coriolis, baroclinic pressure gradient, advection, viscosity and surface forcing²) except the SSH pressure force. Tracer turbulent fluxes (diffusion) and surface flux are not considered here but can be easily added to the right hand side of (3). Note that the free surface has not been linearized—the time varying ocean thickness $h = H + \eta$ is used within the divergence

¹ Viscous terms are generally included and dissipate the total energy in a significant way. This reduces the concern about energy conservation of the non-viscous case.

² The momentum flux associated with precipitation and evaporation is generally expressed as $Pv_{\text{rain}} \simeq Pv_{\text{surf}}$. This matches the lateral velocity of the rain, v_{rain} , with the surface ocean velocity, v_{surf} , as discussed by Griffies et al. (2001); it is included here in the \mathbf{G}_v term.

of the flow (1). Eqs. (1)–(3) are the flux form of the shallow-water equations which implicitly contain the kinematic boundary conditions (see for e.g. Griffies et al., 2001, p. 1090).

Using the finite volume method to discretize (3) ensures a global conservation of tracer T , since the global integral of $\nabla \cdot (hT\mathbf{v})$ vanishes with no normal flow boundary conditions. The evolution of the global tracer content is simply equal to the integrated surface flux. Providing (1) and (3) are discretized in the same way, both in time and space, a uniform concentration T_0 will remain constant (since Eqs. (3) and (1) differ by only a constant factor T_0), and the model will conserve any tracer locally.

To satisfy this criteria, we discretize Eqs. (1) and (3) in time using the forward scheme:

$$(h^{n+1} - h^n)/\Delta t = -\nabla \cdot h^n \mathbf{v}^n + P^n \quad (4)$$

$$(h^{n+1} T^{n+1} - h^n T^n)/\Delta t = -\nabla \cdot h^n T^n \mathbf{v}^n + (PT_{\text{rain}})^n. \quad (5)$$

The stability of such a scheme relies on the choice of spatial discretization and will be addressed later. The formulation that Griffies et al. (2001) described follows the same general idea but the leap-frog scheme makes it slightly more complex and also requires a time filtering leading to a compromise between local and global conservation.

The same forward time stepping applied to the gravity wave term in the momentum Eq. (2) would be unstable unless a very small time step is used. For this reason, ocean general circulation models (OGCM) treat the time stepping of the free-surface equations differently from the rest of the model; for instance, the split-explicit method (Killworth et al., 1991; Griffies et al., 2001), the filtering method (Roullet and Madec, 2000) or, as we consider here, the implicit method (Dukowicz and Smith, 1994; Marshall et al., 1997b). As proposed by Dukowicz and Smith (1994), a part γ (with $0 \leq \gamma \leq 1$) of the surface pressure gradient in Eq. (2) and a part β (with $0 \leq \beta \leq 1$) of the divergence of the barotropic flow in Eq. (1) are evaluated at time level $n + 1$, thus:

$$(\mathbf{v}^{n+1} - \mathbf{v}^n)/\Delta t = \mathbf{G}_v^{n+1/2} - g\nabla[\gamma\eta^{n+1} + (1 - \gamma)\eta^n] \quad (6)$$

$$(\eta^{n+1} - \eta^n)/\Delta t = \beta(P - \nabla \cdot h\mathbf{v})^{n+1} + (1 - \beta)(P - \nabla \cdot h\mathbf{v})^n \quad (7)$$

The motivations for introducing the variable η (Eq. (7)) for the free-surface elevation in addition to the column thickness h (Eq. (4)) is discussed later. The following choices of β and γ are of particular interest:

- $(\beta, \gamma) = (0, 1)$ or $(1, 0)$ leads to an explicit scheme which is stable only for a small Δt that resolves the external gravity waves.
- $(\beta, \gamma) = (1, 1)$ corresponds to the original (Marshall et al., 1997a) implicit free surface method with backward time stepping. It is unconditionally stable, damping the energy associated with unresolved (fast) external modes.
- $(\beta, \gamma) = (1/2, 1/2)$ corresponds to Crank–Nicolson time stepping that conserves the total energy and remains stable without a limitation on time step. The energy of unresolved (fast) modes is aliased onto slower modes.

Since Eqs. (4) and (7) are two discrete formulations of (1), η and h must not be allowed to evolve independently. Rather than integrating (4) and (7) separately and allowing truncation error to accumulate and cause the evolution of η and h to diverge, we impose:

$$\eta^n + H = (1 - \beta)h^n + \beta h^{n+1} \quad (8)$$

in agreement with (4) and (7). Using Eqs. (4) and (8) we can replace (7) by:

$$\eta^{n+1} = (h^{n+1} - H) + \Delta t \beta (P - \nabla \cdot h \mathbf{v})^{n+1} \quad (9)$$

Then Eqs. (6) and (9) are combined, using (6) to substitute for \mathbf{v}^{n+1} in (9):

$$\eta^{n+1} - \beta \gamma \Delta t^2 \nabla \cdot h^{n+1} \mathbf{g} \nabla \eta^{n+1} = (h^{n+1} - H) + \beta \Delta t P^{n+1} - \beta \Delta t \nabla \cdot h^{n+1} \mathbf{v}^* \quad (10)$$

with

$$\mathbf{v}^* = \mathbf{v}^n + \Delta t \mathbf{G}_v^{n+1/2} - (1 - \gamma) \Delta t \mathbf{g} \nabla \eta^n$$

and

$$\mathbf{v}^{n+1} = \mathbf{v}^* - \gamma \Delta t \mathbf{g} \nabla \eta^{n+1} \quad (11)$$

The method is the following: (a) (4) and then (5) are solved explicitly, using an appropriate stable advection scheme for (5). (b) $\mathbf{G}_v^{n+1/2}$ is evaluated either using the density field at time level n (synchronous time step) or at level $n + 1$ (staggered time step). (c) The implicit Eq. (10) is solved for η^{n+1} and (d) \mathbf{v}^{n+1} is derived from (11).

Having two variables η and $h - H$ each representing the surface displacement allows a separate time stepping of the model cell thickness h and the dynamic surface elevation η . This is essential for ensuring exact conservation of tracers, using h in the volume and tracer transports (4 and 5), and a stable scheme for external gravity waves when solving the free-surface Eqs. 6 and 7. Furthermore, since h (instead of $H + \eta$) appears inside the divergence of the volume transport (in the right-hand-side of Eq. (7)) the free-surface Eq. (10) remains linear in η^{n+1} and can be easily treated implicitly. Without any approximation, this method overcomes the difficulties related to the non-linear term inside the free-surface equation that Griffies et al. (2000) mentioned as a limitation of the implicit method.

The non-linear free surface introduces only minor changes to the code: the divergence of the column integrated flow is computed at the beginning of the time step to evaluate h^{n+1} (4). The NLFS formulation uses h^{n+1} in several places, in particular to update the surface level thickness, both at tracer points and at the u and v points of the C-grid. Note that since a finite volume discretization is also used for the momentum equation, most of the tracer conservation properties are also inherited for momentum.

To find the surface pressure, the solver matrix must be computed at each time step because it now contains the total water column thickness (h^{n+1} on the left hand side of Eq. (10)) in place of the fixed ocean depth H in the original linearized free surface form. The conjugate gradient preconditioner (Marshall et al., 1997a) is evaluated from the initial matrix (computed from H) and kept unchanged, since updating the preconditioner using the updated matrix shows no significant improvement in the convergence speed of the solver. Globally, the NLFS induces only a marginal increase in computer time (4% of the total computer time for the simple test presented in Section 5.2).

The effects of the Crank–Nickelson barotropic time stepping ($\beta = \gamma = 1/2$) on the model efficiency is ambiguous: Compared to the backward time stepping, the global model is slightly faster with Crank–Nickelson stepping if the same time step is used since less solver iterations are

necessary to reach the same precision level. However, one might be able to use a longer time step with the backward time stepping since it damps high frequencies and could eventually increase the model stability.

3. Implementation with the Lax–Wendroff scheme for tracers

In the previous section, a general method was set out that conserves tracers with a two time-level scheme. However, the stability, accuracy and effective conservation of the scheme depends on details of the discretization in space, which we now present here.

The spatial discretization uses the finite volume method that ensures global conservation of volume and tracers (Marshall et al., 1997a). Advective terms take the form of a divergence of an advective flux $\nabla_{3d} \cdot T\mathbf{v}$ integrated over a finite volume $h^n \Delta x \Delta y$:

$$-\delta_i F_x^n - \delta_j F_y^n - \delta_k F_z^n$$

Δx , Δy are the grid spacing in the corresponding x , y direction with (i, j, k) the space indices and (u, v, w) the velocity components in respectively the x , y , z directions. The area integrated fluxes, F_x , F_y , F_z , are evaluated at each tracer cell interface:

$$\begin{aligned} F_{x,i+1/2} &= \Delta y \cdot h_{i+1/2} \cdot u_{i+1/2} \cdot \bar{T}_{i+1/2}^i \\ F_{y,j+1/2} &= \Delta x \cdot h_{j+1/2} \cdot v_{j+1/2} \cdot \bar{T}_{j+1/2}^j \\ F_{z,k+1/2} &= \Delta x \cdot \Delta y \cdot w_{k+1/2} \cdot \bar{T}_{k+1/2}^k \end{aligned} \quad (12)$$

The C-grid directly provides $u_{i+1/2}$ at the tracer cell interface. We invoke the analogue of a partial cell (as for the bottom cell thickness, see Adcroft et al., 1997) to represent the variable surface cell thickness. We set $h_{i+1/2}^n = \min(h_i^n, h_{i+1}^n)$, as proposed by Griffies et al. (2001). The volume transport $\Delta y \cdot h_{i+1/2} \cdot u_{i+1/2}$ is discretized in the same way as tracer fluxes, and is used in the continuity Eq. (4) to derive h^{n+1} and the vertical velocity. The original model formulation already contains a non-uniform cell thickness to represent partial cell thickness (Adcroft et al., 1997) so that the time varying surface layer thickness can be added with only minor modifications and no significant computational cost.

The tracer value at the interface, $\bar{T}_{i+1/2}^i$, is defined according to the advection scheme. Following the previous section, we use a forward two time-level scheme. Several conservative schemes of this kind have been recently implemented in the MITgcm (Adcroft et al., 2002). Here we will only refer to the simplest one, the Lax–Wendroff scheme, in which $\bar{T}_{i+1/2}^i$ in Eq. (12) is given by:

$$\bar{T}_{i+1/2}^i = (T_i + T_{i+1})/2 + \frac{u \cdot \Delta t}{\Delta x} (T_i - T_{i+1})/2$$

This provides a stable second order accurate (in both time and space) advection scheme.

4. Implementation using Adams–Bashforth time stepping

The original MITgcm model (Marshall et al., 1997a) uses the Adams–Bashforth time stepping (AB) to integrate the equations of motion forward in time. The general method outlined in Section 2 must be adapted to work with a three time-levels scheme like the AB.

The NLFS implementation is presented as a modification of the original, linear free-surface model. This implementation offers several advantages such as clear backward compatibility with the linear free-surface (linear FS) code and a flexible choice between the linear and NLFS. This flexible switch between the two forms can even be made locally and temporary if necessary. For example, in simulations with high vertical resolution, the free surface displacement can occasionally become as large as the first level thickness but negative. A NLFS simulation would be terminated since vanishing grid cells cannot yet be handled. Instead, a minimum thickness can be imposed and the part of $\partial\eta/\partial t$ that has not been taken into account in the cell thickness variation is treated as in the linear FS approximation. From a practical point of view, this allows one to use the NLFS option in a safe way and with no restriction on vertical resolution near the surface. These advantages motivate the present choice. We first present details of the original linear FS formulation which relate to tracer conservation and then describe the NLFS implementation as a modification of it.

In the original linear FS model, the tracer discretization is based on a second order, centered in space advection scheme, with a second order AB:

$$T^{n+1} = T^n + \frac{\Delta t}{H} G_{AB}^{n+1/2} + \Delta t F_{\text{forcing}}^n \tag{13}$$

with

$$G_{AB}^{n+1/2} = (1 + \epsilon_{AB})G^n - \epsilon_{AB}G^{n-1}$$

where G contains advection (and some diffusion) terms whereas the forcing (including fresh water flux and remaining diffusion terms) are kept outside of Adams–Bashforth. The AB parameter $\epsilon_{AB} = 1/2$ ensures true second order precision in time, but for stability reasons, a slightly higher value is generally used (e.g. $\epsilon_{AB} = 0.6$ for the test cases presented in the next section).

Using the same simplified notation of Section 2 (single layer), the general form of the G term is: $G = -\nabla \cdot (HT\mathbf{v})$ with a centered in space expression ($\bar{T}_{i+1/2}^i = (T_i + T_{i+1})/2$) for the flux (12) (see Section 3 for more details). However, with the linear FS, because the surface level thickness is kept constant while the SSH is moving, a “surface correction”³ is added in the flux form formulation. This surface correction corresponds to the tracer flux associated with the top vertical velocity $w_s \cdot T_1$ where T_1 is the tracer concentration of the uppermost level and w_s is defined as the convergence of the vertically integrated volume transport: $w_s^n = -\nabla \cdot H\mathbf{v}^n$. The full expression for G then becomes:

$$G^n = -\nabla \cdot HT^n\mathbf{v}^n - w_s^n T_1^n \tag{14}$$

The “surface correction” guarantees local conservation, but breaks global conservation since $\int \int_{\mathcal{A}} w_s T_1 d\mathcal{A}$ is generally non-zero (although $\int \int_{\mathcal{A}} w_s d\mathcal{A} = 0$). On the one hand, the fast adjustment of the SSH (e.g., after a convective adjustment) combined with high background tracer concentration (e.g., around 35 psu for the salinity, or around 300 K for the absolute temperature) can generate serious local problems if the “surface correction” is not included, since the departure

³ An alternative interpretation of the linearized free-surface approximation is to consider the model domain ($-H < z < 0$) as a truncation of the full one ($-H < z < \eta$) so that the surface correction appears naturally as the advective flux of tracer through the open boundary at $z = 0$.

from the local conservation rule is precisely the correction term $w_s T_1$. On the other hand, the mismatch in the global tracer content associated with this surface correction is generally small and given by:

$$\mathcal{V} \Delta \bar{T} = \mathcal{V} \bar{T}^{n+1} - \mathcal{V} \bar{T}^n = -\Delta t \int \int_{\mathcal{A}} [(1 + \epsilon_{AB})(w_s T_1)^n - \epsilon_{AB}(w_s T_1)^{n-1}] d\mathcal{A}$$

where \mathcal{A} , \mathcal{V} are the ocean area and volume respectively and \bar{T} is the global mean tracer concentration.

For these reasons, most linear FS models that use a finite volume tracer discretization incorporate such a surface correction (Marshall et al., 1997a; Roulet and Madec, 2000; Griffies et al., 2001).

In the implementation of the NLFS, the general method presented in Section 2 is adapted to deal with the original AB scheme. Using (4) and defining ⁴ $w_s^n = -\nabla \cdot h^n \mathbf{v}^n$, Eq. (5) is equivalent to:

$$T^{n+1} = T^n + \frac{\Delta t}{h^{n+1}} [-\nabla \cdot h^n T^n \mathbf{v}^n - w_s^n T_1^n + P^n (T_{\text{rain}} - T_1)^n] \quad (15)$$

Eq. (15) is close to the original (linear FS) AB formulation ((13) and (14)) and allows us to introduce the AB time stepping as follows:

$$T^{n+1} = T^n + \frac{\Delta t}{h^{n+1}} [G_{AB}^{n+1/2} + P^n (T_{\text{rain}} - T_1)^n]$$

and

$$G^n = -\nabla \cdot h^n T^n \mathbf{v}^n - w_s^n T_1^n \quad (16)$$

with

$$G_{AB}^{n+1/2} = (1 + \epsilon_{AB})G^n - \epsilon_{AB}G^{n-1}.$$

Using Eq. (4), this yields:

$$\begin{aligned} (h^{n+1} T^{n+1} - h^n T^n) / \Delta t &= -(1 + \epsilon_{AB}) \nabla \cdot (h T \mathbf{v})^n + \epsilon_{AB} \nabla \cdot (h T \mathbf{v})^{n-1} + (P T_{\text{rain}})^n \\ &\quad - \epsilon_{AB} [(w_s T_1)^n - (w_s T_1)^{n-1}] \end{aligned} \quad (17)$$

This formulation has several advantages:

1. The same formulation can be used with both AB and forward two time-level (e.g., Lax–Wendroff) time stepping: one recovers (15) by simply replacing $G_{AB}^{n+1/2}$ in (16) by G^n computed with Lax–Wendroff fluxes (12). This returns the fully conservative scheme described in Section 2 since (5) is equivalent to (17) with $\epsilon_{AB} = 0$. This formulation is also close enough to the original formulation to involve only slight modifications in the code and to allow a switch back to the linear FS option.
2. It is clear from (16) that the surface-level expansion/contraction term ($w_s T_1$) inside the “ G^n ” term ensures a precise local conservation, just as the surface correction does in the linear FS case. The reasons that motivate adding this surface level expansion term in G^n for the non-lin-

⁴ Note that w_s is not the vertical velocity at the surface. This later quantity is given by: $w_{z=\eta} = w_s + \mathbf{v}_{z=\eta} \cdot \nabla \eta$.

ear case are similar to those given for the surface correction in the linear FS case. Since SSH can exhibit fast variations, with the possibility of sign changes from one time step to the next, the amplitude of the local surface term (i.e. the last term in Eq. (17)) can be of the same order as the surface correction $(w_s T_1)^n$ in the linear FS formulation. It therefore needs to be included in the tracer Eqs. (16) and (17).

3. This formulation does not exactly conserve the global tracer content between time-steps, since the contribution of the surface level expansion term does not integrate to zero:

$$(\mathcal{V}\bar{T})^{n+1} - (\mathcal{V}\bar{T})^n = -\epsilon_{AB} \int \int_{\mathcal{A}} [(w_s T_1)^n - (w_s T_1)^{n-1}] d\mathcal{A} \neq 0.$$

However, this equation can be rearranged so that the global quantity

$$(\mathcal{V}\bar{T}^*)^{n+1} = \int \int_{\mathcal{A}} [(hT)^{n+1} + \epsilon_{AB}\Delta t (w_s T_1)^n] d\mathcal{A} \tag{18}$$

appears to be exactly conserved. Furthermore, this “modified” global tracer content $\mathcal{V}\bar{T}^*$ is a good approximation to the total tracer content $\mathcal{V}\bar{T}$ since $\epsilon_{AB}\Delta t \int \int_{\mathcal{A}} w_s T_1 d\mathcal{A}$ is generally very small. Therefore, the exact conservation of $\mathcal{V}\bar{T}^*$ guarantees that the model tracer content cannot drift.

4. For the purpose of checking tracer conservation, inaccuracy in local conservation is relatively difficult to isolate whereas global conservation is easily diagnosed. Since our formulation exactly satisfies local conservation, we can evaluate the error in global conservation and provide estimates of the accuracy of the method. This is done in the next section.

5. Illustrative examples of property conservation

This section illustrates how the NLFS formulation previously described improves the conservation of various quantities, such as volume, temperature, salinity with time varying fresh water forcing, and finally energy. Since NLFS effects are generally relatively small in the global ocean and difficult to isolate, here we consider only ideal tests with very simple geometry and concentrate on free surface effects. A steady state problem like the Goldsbrough–Stommel circulation described by Huang (1993) is not a selective test to address tracer conservation regarding the time stepping. For this reason, we prefer to include a strong time dependency in the test experiment presented here. This is achieved by imposing a strong time dependent forcing or posing an initial adjustment problem.

The first test case is an ocean wind driven gyre circulation similar to the problem described analytically by Stommel (1948). The ocean depth is relatively shallow ($H = 400$ m) to emphasize NLFS effects which scale like η/H . There are four vertical levels each of 100 m. The domain is 59° wide in longitude and extends from the Equator to 59° N on a spherical $1^\circ \times 1^\circ$ grid. The horizontal and vertical viscosity are 400 and 10^{-2} m²/s respectively, and the same values are used for diffusivity. The time step is set to $\Delta t = 20$ min. The initial state is at rest, horizontally uniform and thermally stratified $\theta = 20, 16, 12, 8$ [°C]. Salinity is initially uniform ($S_0 = 33$ psu) and has no influence on density which is assumed to be only function of the potential temperature θ : $\rho = \rho_0(1 - \alpha\theta)$ with $\alpha = 2 \times 10^{-4}$ °C⁻¹. A constant zonal wind stress is applied $\tau_x = \tau_0 \sin(\pi\varphi/L_\varphi)$ with $\tau_0 = 0.1$ Nm⁻², φ the latitude and L_φ the domain latitudinal extension (59°).

In addition, a relatively strong fresh water forcing ($E - P$) is added in the South-West corner that peaks at 1.5 m/day and linearly decreases toward the East and toward the North:

$R_0 = [16 - \varphi - \lambda] \cdot 0.1$ m/day (λ, φ in° and $R_0 \geq 0$), with a simple diurnal cycle: $E - P = R_0 \sin(2\pi t/1\text{day})$. It can be treated as a real fresh water flux (“Real FW”) (+ = out off the ocean) with the NLFS or converted to an equivalent salt flux (“Salt Flx”): $Flx_S = S_c \cdot (E - P)/\Delta z_1$ (here $S_c = 35$ psu) without direct effects on the SSH. In the case of the linear free surface, a “virtual fresh water” (“Virtual FW”) formulation can be defined, where $E - P$ directly affects the SSH (as in real fresh water input) but needs to be converted to an equivalent salt flux to have an impact on the salinity, since the thickness of the first layer is kept fixed (and consequently also the ocean volume \mathcal{V}). Table 1 provides a summary of these different options.

The fast variations of $E - P$ allow one to check salt conservation when using various time stepping schemes; in the absence of thermal forcing, this simple case provides a good test of global and local conservation of θ during the initial adjustment of the SSH under the wind forcing. Note that the dilution effect on salinity is present in all experiments (with real FW, virtual FW or salt Flx) but is decoupled from the dynamics since $\partial\rho/\partial S = 0$. The fresh water impact on the dynamics is limited to the direct effect on SSH and is only present when real FW or “virtual” FW is applied (Table 2, exp. 0, 5, 6, 9 and 10).

5.1. Volume conservation

The model exactly conserves volume in all cases, whether linear or NLFS, and whether backward ($\beta = \gamma = 1$) or Crank–Nickelson ($\beta = \gamma = 1/2$) time stepping of the free-surface equations.

With no real fresh water input, the average SSH remains equal to zero during a five days simulation with a deviation of less than 2×10^{-16} m, the level of computer precision. During the same period, the SSH range (maximum–minimum) increases to 0.3 m. In the original formulation, volume conservation is less precise: after five days, the average SSH is -7×10^{-16} m (Fig. 1a) but it drifts between -2 and -3×10^{-12} m over 10 years (Fig. 1b). With the new implementation, the mean SSH remains zero with the same accuracy (few 10^{-16} m) over 10 years using equivalent options (backward time stepping and linear free-surface). The explicit integration of the continuity equation (see details in Appendix A) prevents truncation and solver errors from accumulating. From here on we only consider the new formulation that exactly conserves the volume.

Several experiments of five day duration have been conducted with various combinations of options, to test the robustness of the tracer conservation. The evolution of the global mean, the lowest and highest values of the SSH is plotted in Fig. 2a–c respectively, and correspond to four experiments (Table 2, exp. 3, 4, 5 and 6) that use different options: the free surface time stepping is

Table 1
Free surface formulation and fresh water treatment

Free surface equation	Salinity equation	Label	
$\partial_t \eta + \nabla \cdot (H + \eta) \mathbf{v} = P$	$\partial_t (hS) + \nabla \cdot hS \mathbf{v} = 0$	NL FS	Real FW
$\partial_t \eta + \nabla \cdot (H + \eta) \mathbf{v} = 0$	$\partial_t (hS) + \nabla \cdot hS \mathbf{v} = -P \cdot S_c$	NL FS	Salt flux
$\partial_t \eta + \nabla \cdot H \mathbf{v} = 0$	$\partial_t (HS) + \nabla \cdot HS \mathbf{v} = -P \cdot S_c$	Lin FS	Salt flux
$\partial_t \eta + \nabla \cdot H \mathbf{v} = P$	$\partial_t (HS) + \nabla \cdot HS \mathbf{v} = -P \cdot S$	Lin FS	Virtual FW

Table 2

Accuracy of the global conservation of heat and salt using various combination of options relative to the free surface treatment and the tracer advection scheme.

Experiment number and options					Global mean deviation	
<i>N</i>	Linear/Non	Flux	FS stepping	Advection	$\Delta\theta$ (°C)	ΔS (psu)
0	Lin FS	Virtual FW	Back	LW	5×10^{-7}	7×10^{-6}
1	Lin FS	Salt Flx	Back	LW	2×10^{-7}	2×10^{-7}
2	Lin FS	Salt Flx	CrNi	LW	2×10^{-7}	4×10^{-7}
3	NL FS	Salt Flx	Back	LW	0	1×10^{-12}
4	NL FS	Salt Flx	CrNi	LW	0	1×10^{-12}
5	NL FS	Real FW	Back	LW	0	2×10^{-12}
6	NL FS	Real FW	CrNi	LW	0	2×10^{-12}
7	Lin FS	Salt Flx	Back	AB	2×10^{-7}	2×10^{-7}
8	NL FS	Salt Flx	Back	AB	3×10^{-9}	6×10^{-9}
9	NL FS	Real FW	Back	AB	2×10^{-8}	9×10^{-8}
10	NL FS	Real FW	CrNi	AB	3×10^{-8}	1×10^{-7}

either implicit (exp. 3 and 5) or Crank–Nickelson (exp. 4 and 6); the fresh water forcing is either real FW (exp. 5 and 6) or converted to salt flux (exp. 3 and 4).

In our experiments, the dynamical behavior of the SSH is not sensitive to the tracer advection scheme or whether the free surface is linear or non-linear and so only four experiments among the 11 listed in Table 2 are shown in Fig. 2, all 4 using NLFS with Lax–Wendroff advection scheme.

The global mean SSH exactly match the integrated fresh water input or remains flat when salt flux is used. Under wind stress forcing, the SSH slowly builds up low and high large scale surface pressure patterns (Fig. b, c, exp. 3 and 4). Superimposed on this slow tendency, strong, local real fresh water forcing (exp. 5 and 6) generates local excursions of SSH that are of the same magnitude (around 0.3 m) as the wind driven adjustment after five days. Using a Crank–Nickelson time stepping produces slightly higher SSH standard deviation (in space) and larger SSH excursions than the implicit scheme. This is related to the damping properties of the backward time stepping procedure and will be discussed in sub-section (c).

5.2. Tracer conservation

Tracer conservation is expressed differently according to the boundary condition used for $E - P$: with real fresh water input, the ocean volume \mathcal{V} changes but the total salt content $\mathcal{V}\bar{S}$ remains constant. The total heat content can change because the water input enters or leaves the surface with temperature θ_{rain} that is usually equal to the local surface temperature. Here, for simplicity, we set $\theta_{\text{rain}} = 14$ °C which also corresponds to the global mean initial temperature ensuring that global mean temperature is conserved. When salt flux or “virtual fresh water” flux are used, the volume is constant and the global mean temperature is also unchanged. In this case, the global mean salinity follows the time and space integrated salt flux:

$$\bar{S}_{\text{FS}}(t) = \bar{S}_0 + \frac{S_c}{\mathcal{V}} \int_0^t \left[\int \int_{\mathcal{A}} (E - P) d\mathcal{A} \right] dt$$

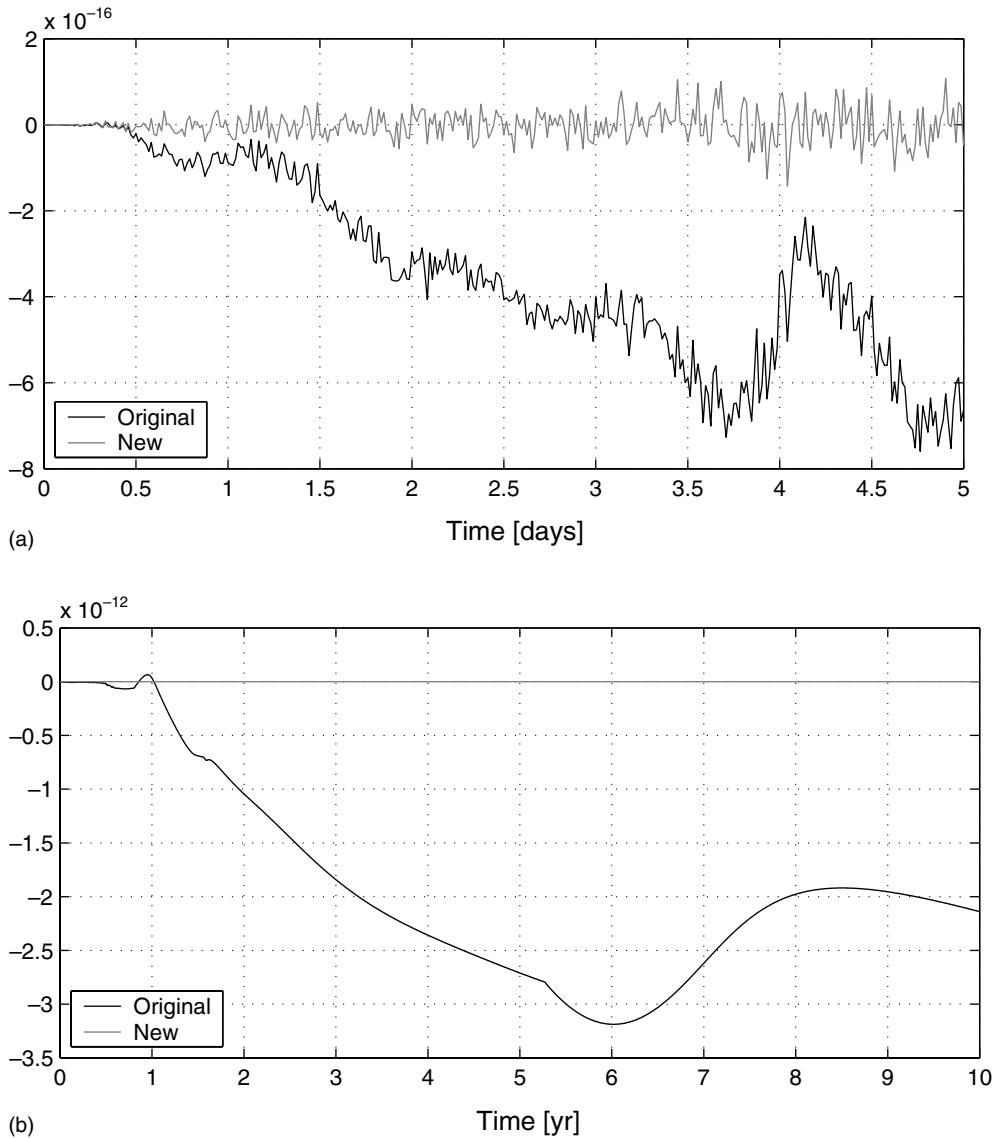


Fig. 1. Evolution of the global mean SSH (m) with the original model (back line) and the new formulation (gray line) which includes an explicit integration of the continuity equation (see Appendix A). The linear free-surface with backward time stepping is used without fresh water input. Fig. 1a (top) corresponds to the first five days of the simulation that has been extended up to 10 years (Fig. 1b, bottom).

The degree of conservation is expressed in both cases in terms of global mean temperature deviation: $\Delta\theta = \bar{\theta} - \bar{\theta}_0$ and equivalent mean salinity deviation: $\Delta S = \bar{S}\mathcal{V} / \mathcal{V}_0 - \bar{S}_{\text{ref}}$ corresponding to the global salt content minus the theoretical value $\bar{S}_{\text{ref}} = S_0$ or $\bar{S}_{\text{ref}} = \bar{S}_{\text{Fxs}}(t)$.

The range of variations (maximum ΔT minus minimum ΔT) of temperature and salinity are gathered in Table 2. The computer precision is such that the accuracy of integrated quantities, for example the mean salinity, cannot be better than 10^{-12} .

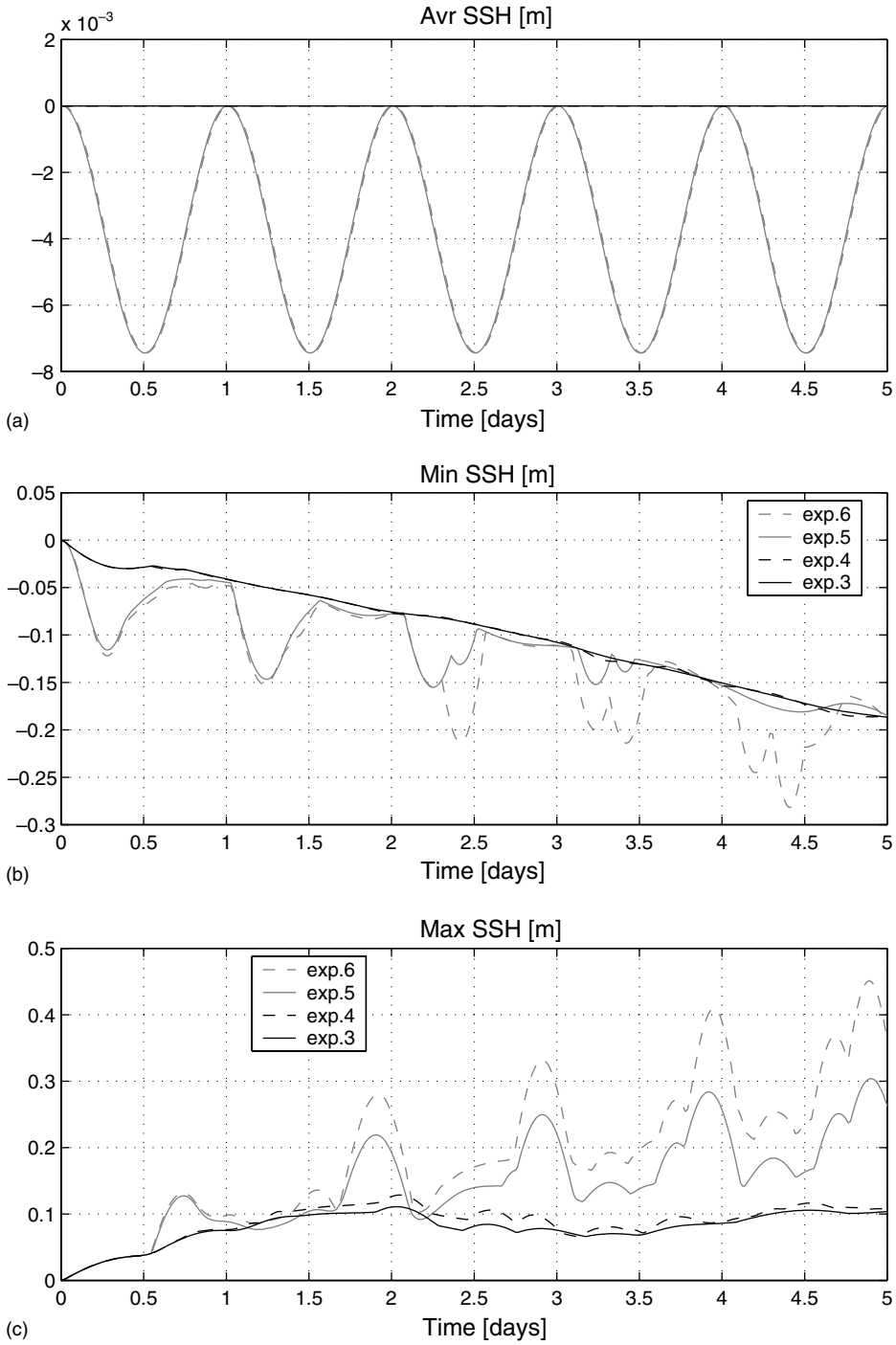


Fig. 2. Evolution of mean (Fig. 2a, top), minimum (Fig. 2b, middle) and maximum (Fig. 2c, lower) of the SSH [m] over the full domain. Results of four experiments are plotted: exp. 3, continuous black line; exp. 4, dash black line; exp. 5, continuous gray line; exp. 6, dash gray line.

The first set of experiments (exp. 0–6) uses the forward Lax–Wendroff scheme and confirms the exact conservation of heat and salt of the NLFS implementation, with or without real fresh water input. By contrast, the LinFS formulation exhibits small deviations ($\sim 10^{-7}$) for both temperature and salinity (Fig. 3a,b). These are associated with the integrated “surface correction” term $-w_s T_s$ (see Section 4). The area integrated surface correction is relatively small but can accumulate in time and may produce a significant drift, as in experiment 0 (Fig. 3c) in which the mean salinity decreases by 7×10^{-6} psu in five days, corresponding to 0.5×10^{-3} psu/yr.

The reason for the large drift in exp.0 is the presence of the strong diurnal cycle of $E - P$ that directly affects the SSH (“virtual fresh water” flux), whereas the other LinFS experiments use only salt flux. During the first half of the day, $E - P > 0$ is applied to the SSH and adjustment of the barotropic flow results in convergent motion, positive w_s and a large negative surface correction $-w_s S_1$, since S_1 is locally larger than the mean salinity due to $E - P$ effects. When $E - P$ reverses during the second half of the day, the surface correction becomes positive but smaller than the amplitude of the negative peak, since advection and diffusion processes have already eroded the salinity maxima. While w_s is globally balanced at each time step and locally balanced over a one day period, the two half-day contributions of the surface correction term do not balance $(-w_s S_1)^- + (-w_s S_1)^+ < 0$, and the net integral effect over one diurnal cycle is clearly negative, resulting in a negative drift of the mean salinity (Fig. 3c).

The second set of experiments (exp. 7, 8, 9 and 10) uses the three time-level Adams–Bashforth advection scheme, and yields non-exact global conservation (Table 2). The conservation is better with the NLFS formulation than with the linear free surface, especially when the comparison is restricted to identical $E - P$ forcing experiments, (exp. 8 versus 7). Note that exp. 9 can also be compared to exp. 0 since this later experiment has been repeated using the AB scheme and yields the same salinity and temperature drift as exp. 0.

The NLFS conservation is not only more accurate than the linear one, but also improved qualitatively: the tracer deviation does not drift with NLFS but tends to remain around the zero line. This is specially true in experiment 9 (or 10) which incorporates real fresh water input and exhibits relatively high temperature and salinity deviations compared to other NLFS simulations (Table 2). However the deviation always returns to almost zero at the end of each day (Fig. 3a,b). This is in agreement with the “error cancellation” idea developed in Section 4, which prevents any significant drift to develop. This can be differently expressed as the exact conservation of the “modified” global mean temperature $\bar{\theta}^*$ and salinity \bar{S}^* defined according to Eq. (18). In order to precisely check this property, the surface integral of the surface level expansion term: $Se(T) = \Delta t / \mathcal{V} \int \int_{\mathcal{A}} (w_s T_1) d\mathcal{A}$ is computed for temperature ($T = \theta$) and salinity ($T = S$) and the modified global mean tracer concentration derived thus, $\bar{T}^* = \bar{T} + \epsilon_{AB} Se(T)$. Fig. 4 plots the evolution of the temperature deviation $\Delta\theta$, the surface level expansion term $Se(\theta)$ and the modified mean temperature deviation $\Delta\theta^*$ (Fig. 4a) for exp. 8 (equivalent salt flux forcing), and similarly for the salinity ΔS , $Se(S)$ and ΔS^* (Fig. 4b) for exp. 10 (real FW forcing). The SSH variations are only due to wind forcing in exp. 8, and are much weaker than in exp. 10 in which real fresh water is added. Therefore the magnitude of the surface level expansion term is also much weaker in exp. 8 ($\sim 10^{-9}$) than in exp. 10 ($\sim 10^{-7}$) and has no diurnal cycle. Despite those differences, in both experiments the global mean deviation is exactly canceled when the surface level expansion term is added with the Adams–Bashforth factor ϵ_{AB} , resulting in perfect conservation of the modified global mean temperature in exp. 8 and salinity in exp. 10. The agreement is perfect in all the Adams–Bashforth

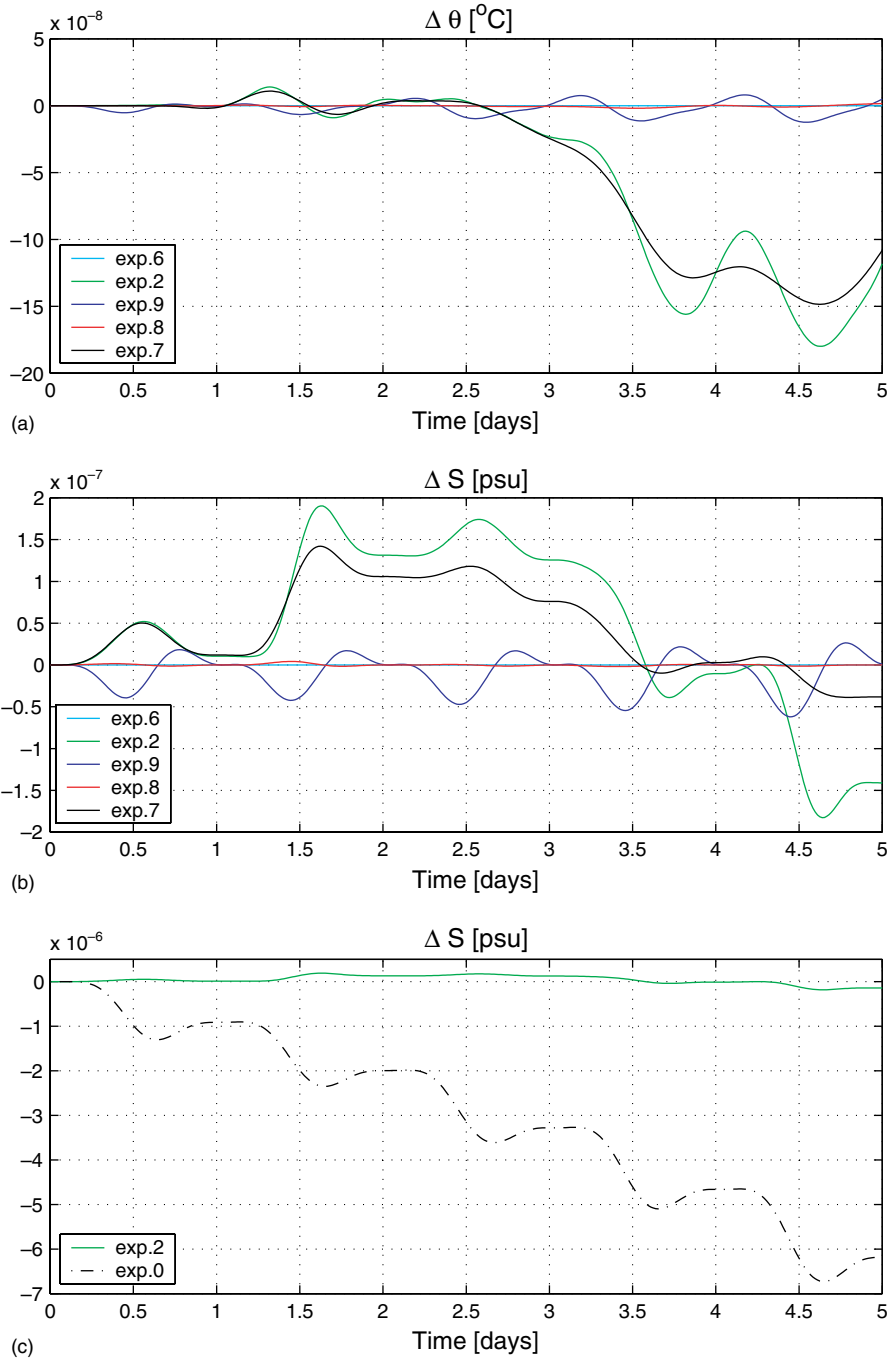


Fig. 3. Evolution of global mean tracer deviation for potential temperature $\Delta\theta$ (Fig. 3a, top) and salinity ΔS (Fig. 3b and c) corresponding to six experiments (see Table 2).

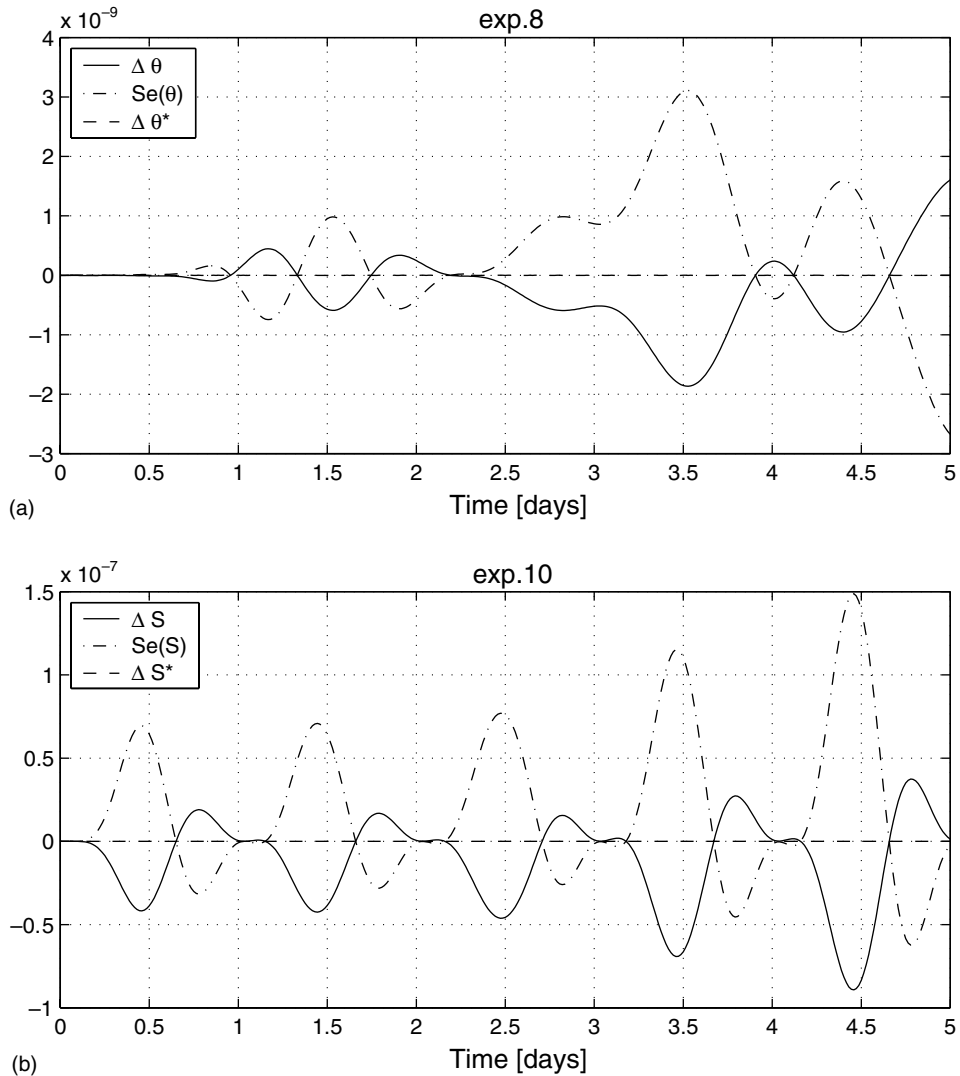


Fig. 4. Conservation of global mean tracer content with NLFS and AB time stepping: the evolution of the global mean deviation ΔT (continuous line), the surface level expansion term $Se(T)$ (dotted line) and the modified global mean tracer T^* (dash line) are plotted for (a) potential temperature in exp. 8 with salt flux and FS backward time stepping (top); and (b) salinity in exp. 10 with real fresh water and FS Crank–Nickelson time stepping (bottom).

NLFS experiments (7, 8, 9 and 10), for both temperature and salinity, within 2×10^{-12} ($^{\circ}\text{C}$ or psu respectively).

From a practical point of view, the exact conservation of \bar{T}^* implies that the global mean tracer concentration is conserved, whatever the length of simulation, to within a factor $\epsilon_{AB}Se(T)$, that is small enough for all practical use of the model. Here in exp. 10, this terms remains smaller than 10^{-7} psu, and given the strong and rapidly varying fresh water forcing, this is probably close to an upper bound.

5.3. Energy conservation

Energy budget analysis can be quiet difficult to carry out in a realistic global ocean model: energy is involved in all ocean processes and altered by numerical details. Therefore, for the purpose of checking the energy conservation of the barotropic dynamics, the model is set up in a very simple configuration. With no forcing and initially at rest, the homogeneous, one layer ocean model adjusts to an initial bump in SSH centered on the equator. The shape of the initial bump is given by $\eta_{t=0} = \Delta h_0 \cdot [1 - \cos(\pi \cdot (1 - r))]/2$ with r the normalized radial distance from the center of the bump: $r = \min(1, \sqrt{x^2 + y^2}/R_{\text{bump}})$; the radius of the bump is $R_{\text{bump}} = 30^\circ$ and the maximum height at the center is $\Delta h_0 = 100$ m. The spherical grid resolution is $2.8125^\circ \times 2.8125^\circ$ and the ocean depth is uniform ($H = 1$ km) and without continents. For simplicity, only non-rotating cases are considered here and the Coriolis parameter is set to zero.⁵ The time step $\Delta t = 450$ s is small enough to resolve external gravity waves at the equator. The small grid spacing near the poles does not limit the time step since both backward or Crank–Nickelson time stepping are unconditionally stable. This is an advantage compared to explicit methods that require a very small time step to satisfy the stability criteria near the poles.

Five different simulations illustrate the evolution of model energy (Figs. 5 and 6). The first experiment (“Back_Lin”) uses the free surface backward time stepping in a pure linear case, i.e., linear free surface with no momentum advection. The remaining four use Crank–Nickelson time stepping, either with the same linear formulation (standard experiment, “CrNi_Lin”), adding only momentum advection (“CN_Ln + Adv”), adding only NLFS effects (“CN_NonLin”) or adding both (“CN_NL + Adv”). For momentum advection, the Adams–Bashforth time stepping is used and for this test ϵ_{AB} is set to 1/2.

The adjustment problem is symmetric with respect to the center of the initial bump so that taking a section across this center provides a good view of a global field. The SSH along the equator is represented in Fig. 5 at time 0, 1.5, 3, 4.5 and 4.72 days of simulation, in the five experiments. In addition, the evolution of global quantities such as the maximum range of SSH (highest point minus lowest point values), the volume mean KE and PE and the mean total energy (PE + KE) is represented in Fig. 6. The volume mean PE and KE are expressed both in m^2/s^2 and computed as follows:

$$PE = \frac{1}{\mathcal{V}} \int \int_{\mathcal{A}} 1/2g\eta^2 d\mathcal{A} \quad \text{and} \quad KE = \frac{1}{\mathcal{V}} \int \int_{\mathcal{A}} h1/2(u^2 + v^2) d\mathcal{A}$$

When the linear free surface approximation is made, the time dependent ocean thickness h is kept constant and set equal to H in the KE expression.

The standard experiment (“CrNi_Lin”) is free of non-linear effects and therefore easier to interpret. The initial SSH anomaly generates gravity waves that propagate in a radial direction

⁵ The simplicity of the non-rotating, purely linear test (detailed in the body of the text) allows one to find an analytical solution using spherical harmonics to verify model results. This also avoids complications concerning the discretization of the Coriolis term on a C-grid, a delicate issue which can have significant impact on energy conservation. Such aspects, although important, go beyond the scope of this paper where we prefer to concentrate on free-surface effects only.

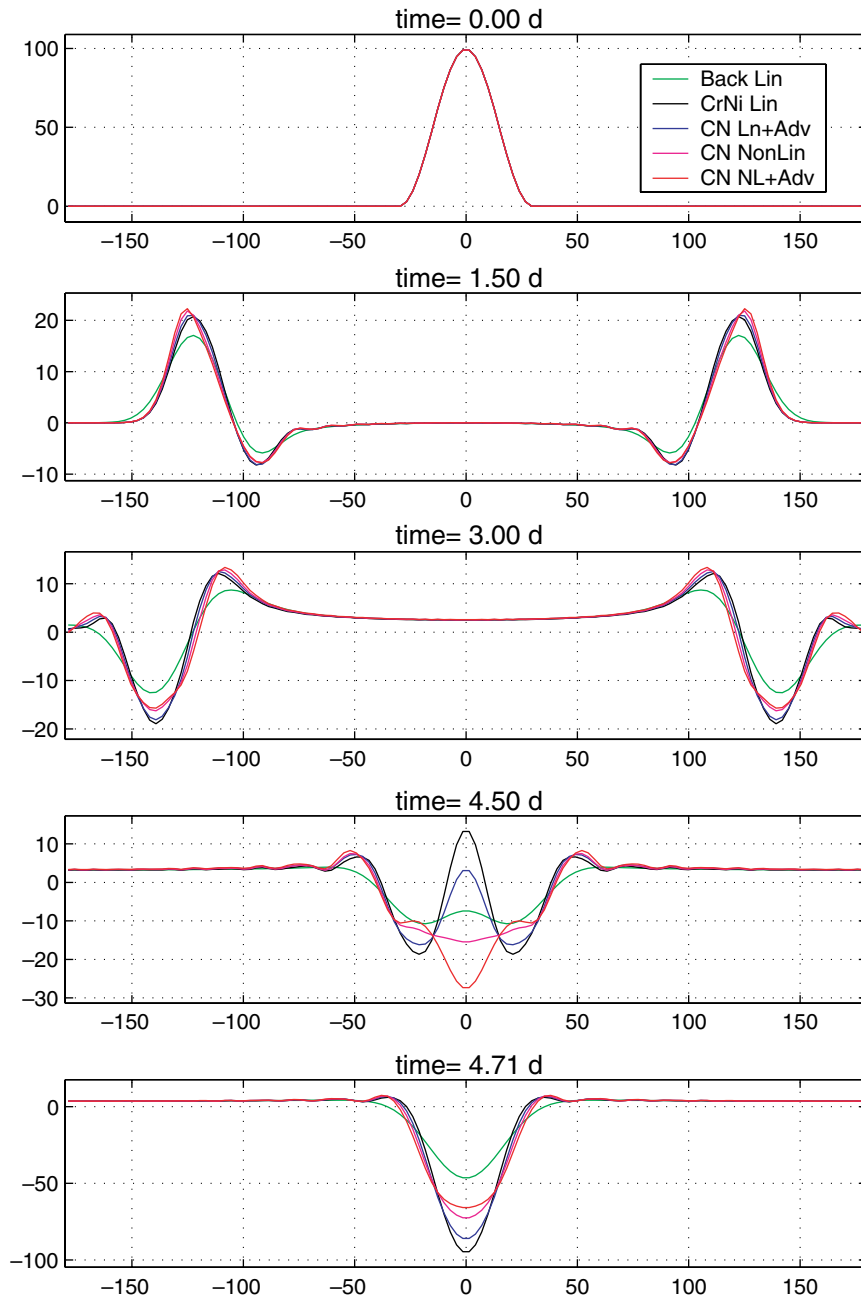


Fig. 5. SSH [m] along the equator corresponding to (from top to bottom) time 0.0, 1.5, 3.0, 4.5 and 4.71 days. Results from five experiments (Back_lin, CrNi_lin, CN_Ln + Adv, CN.NonLin and CN_NL + Adv, see Section 5.3) are plotted.

from the source (Long 0.E) and converge to the symmetric point relative to the sphere center, at 180.E on the equator, before coming back to the source point at time $t = T_{\text{cycle}} \simeq 4.71$ days. T_{cycle} is defined as the time of the first maximum and minimum of, respectively, the mean potential and

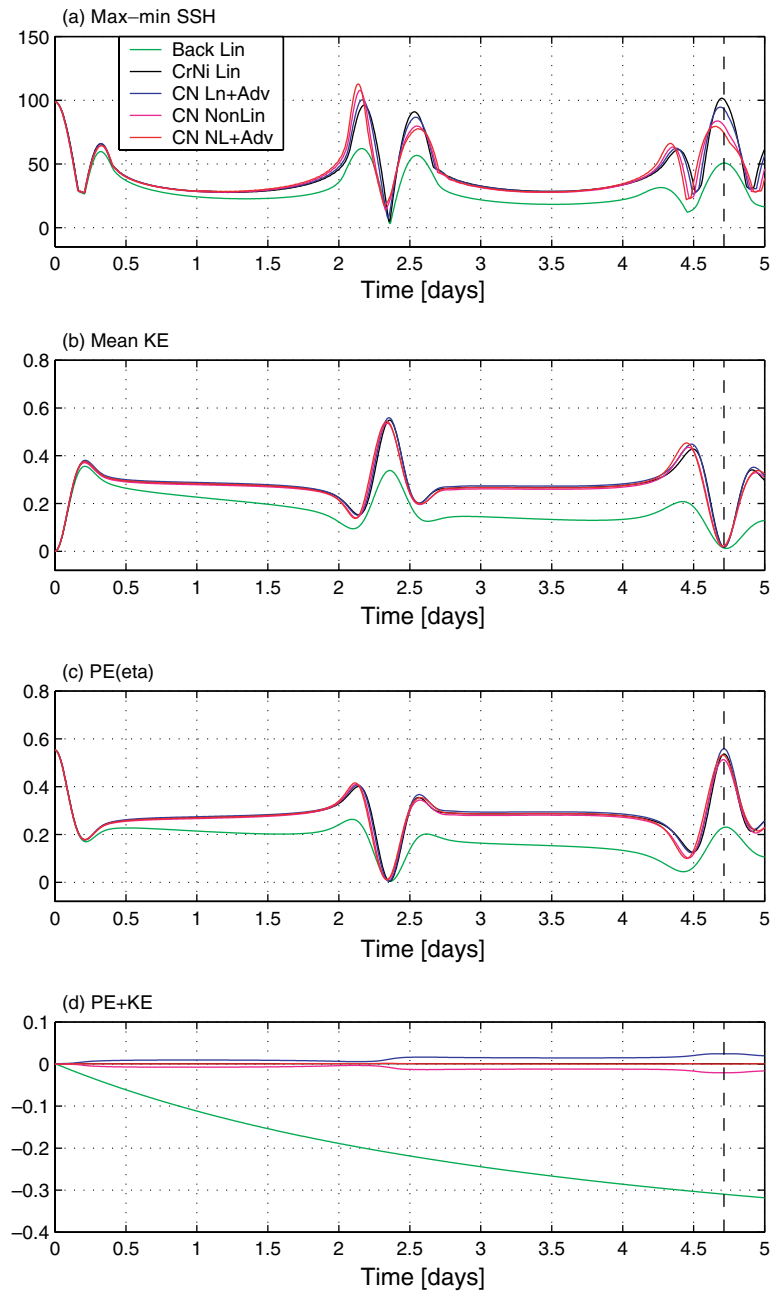


Fig. 6. Evolution of global quantities for five experiments (Back.lin, CrNi.lin, CN.Ln + Adv, CN.NonLin and CN.NL + Adv, see Section 5.3): (a) SSH range (maximum–minimum) [m]; (b) Mean KE [m²/s²]; (c) Mean PE [m²/s²]; (d) Total energy PE + KE deviation from the initial value (0.55375) [m²/s²]. The dash line at $t = 4.71d$ corresponds to the minimum of KE and maximum of PE.

KE, and can be considered as the time period required for the energy to travel around the sphere. T_{cycle} is slightly longer than the period T_0 of non-dispersive plane waves in a cyclic channel: $T_0 = 2\pi R_E / \sqrt{gH} = 4.68d = 112.25h$ with $R_E = 6370$ km the Earth radius. This is due to the dispersive nature of gravity waves on the sphere (Panchev, 1985, p. 179) and also explains the reverse sign of the SSH anomaly after 1 cycle ($t = T_{\text{cycle}}$). The numerical dispersion that mainly affects poorly resolved wave lengths and frequencies is relatively small here, since the shape of the bump is well preserved after one cycle in the pure linear case (Fig. 5d, CrNi_Lin).

Adding momentum advection or relaxing the Linear FS approximation does not change the general behavior of wave propagation but increases the dispersion and results in significant phase differences; this appears clearly on Fig. 5 after 4.5 days of integration. On the contrary, use of backward time stepping (exp = Back_Lin) has only minor phase effects but strongly reduces the amplitude of the SSH anomaly, up to 50% of its initial value after one cycle.

Use of backward time stepping is the largest source of differences in energy evolution (Fig. 6b–d) and maximum range of SSH (Fig. 6a). The damping of fast modes with backward time stepping is responsible for a large decrease in the total energy (more than 50% after four days) (Fig. 6d) and a reduction of the wave amplitude by roughly the same factor. By contrast, non-linear effects on the phase and the shape of the SSH anomalies also modify the evolution of the SSH range but have only a weak influence on the energetics of the system.

The conservation of the total energy is exact in the standard case (no advection of momentum and linear free surface). The departure from the initial value is less than 10^{-13} m^2/s^2 during the whole simulation (five days), at the level of machine precision. Without momentum advection, the NLFS formulation does not conserve the total energy, as shown on Fig. 6d. The departure from the initial value is 0.02 m^2/s^2 (<5% of the total) after five days. This property has been noted before (see e.g., Roulet and Madec, 2000; Griffies et al., 2001) and is related to the coupling of momentum advection and free surface displacement in the KE budget, which can no longer be considered separately, in contrast to the linear FS case. This motivates the inclusion of momentum advection terms in the NLFS experiment CN_NL + Adv and, for comparison, the linear FS experiment CN_Ln + Adv.

Energy conservation is less simple in the presence of momentum advection terms than tracer conservation. Given the objective of this paper, our priority is tracer conservation. Nevertheless, use of the NLFS significantly improves energy conservation; the total energy drifts by less than 1.9×10^{-3} m^2/s^2 in the NLFS case CN_NL + Adv but exceeds 0.02 m^2/s^2 in the linear FS experiment CN_Ln + Adv.

The poor energy conservation of the linear FS case is related to the “surface correction” term, $-w_s \cdot \mathbf{v}$ in the momentum equation that is designed to conserve locally the momentum, whereas global conservation of energy required only half of it. In the NLFS case, a significant improvement in energy evolution can be expected by simply changing the definition of the cell thickness to \bar{h}^i, \bar{h}^j at U,V points; as mentioned by Roulet and Madec (2000), in order to conserve energy an area weighted mean value between the two neighbors must be used $\bar{h}^i = (\mathcal{A}_i h_i + \mathcal{A}_{i+1} h_{i+1}) / 2\bar{\mathcal{A}}^i$ instead of the minimum of the two, to ensure that the time variation of \bar{h}^i corresponds to $\bar{w}_s^i \Delta t$.

With momentum advection and including those two modifications (half of the surface correction in CN_Ln + Adv and modified \bar{h}^i, \bar{h}^j in CN_NL + Adv, hereafter referenced as CN_NL* + Adv, the energy conservation is still not exact, due to the use of Adams–Bashforth for momentum advection. However, the departure from the initial PE remains very small during the

whole simulation (five days); less than $5 \times 10^{-5} \text{ m}^2/\text{s}^2$ and $5.3 \times 10^{-5} \text{ m}^2/\text{s}^2$ in the linear and NLFS experiments respectively. Such small differences are impossible to distinguish from the zero line on Fig. 6d.

In order to assess the magnitude of the total energy drift, the NLFS experiment with modified \bar{h}^i, \bar{h}^j CN_NL* + Adv has been repeated with a small horizontal viscosity $A_h = 1000 \text{ m}^2/\text{s}$, about two order of magnitude smaller than the one currently used in OGCM at the same resolution. The result is a reduction of the total energy of $2.1 \times 10^{-4} \text{ m}^2/\text{s}^2$ after five days, more than four times larger than without horizontal viscosity.

To summarize, apart from the backward time stepping experiment which strongly damps the transient energy, all the Crank–Nickelson tests preserve energy relatively well, but only the pure linear case (linear FS without momentum advection) ensures an exact conservation. When momentum advection is included, the NLFS improves the conservation relatively to the linear FS case, especially when \bar{h}^i, \bar{h}^j are defined in an appropriate manner. Then the residual drift becomes very small, much smaller than the effect of a small horizontal viscosity. This can be unambiguously attributed to the time stepping of momentum advection, since the discretization in space conserves the energy (Adcroft et al., 1997). These results appear to be robust regarding the choice of the time step: using half the time step (225 s) strongly reduces the energy drift of the modified NLFS experiment CN_NL* + Adv by a factor of 6 whereas backward time stepping still results in large energy loss, only 30% smaller than with the standard time step (450 s).

6. Conclusions

A NLFS implementation using the implicit free surface method has been designed to conserve tracer quantities. The conservation is exact when a forward two time-level scheme is used for tracer advection, as in the Lax–Wendroff scheme. When using a three time-level scheme, such as Adams–Bashforth II, the method exactly conserves a modified global tracer content \bar{T}^* that always remains very close to the global mean value \bar{T} . This ensures that the model will not drift during long simulations. The implicit free surface solver can easily accommodate various options (rigid-lid, linear FS, NLFS, non-hydrostatic...) and offers an energy conserving form with a Crank–Nickelson time stepping.

The NLFS method presented here is not radically different from previous studies (Roullet and Madec, 2000; Griffies et al., 2001), but is applied in a different time stepping context. While Griffies et al. (2001) experience some difficulties in ensuring tracer conservation with the leap-frog scheme and time filtering, the time stepping schemes considered here offer the same level of precision (both second order in time and space) and also satisfy tracer conservation.

A simple test illustrates that the NLFS formulation conserves tracers, both locally and globally, and naturally implements fresh water flux. This constitutes an improvement compared to the linear FS formulation. NLFS effects are generally small in full depth ocean models with coarse resolution and slowly varying forcing, but since conservation is easier to implement and more accurate in the presence of NLFS, we prefer it in all calculations.

A simple wave propagation test shows that the free-surface backward time stepping scheme has a large damping effect on the solution which swamps the differences between non-linear and linear FS. Using Crank–Nickelson time stepping exactly conserves the energy of the pure linear model

(linear FS without momentum advection) and allows us to identify NLFS effects on the phase propagation of gravity waves. When momentum advection is included, energy conservation is better with the NLFS formulation than with the linear FS form, and can be further improved with a small modification of the grid interface thickness. However this modification does not induce any noticeable effects on wave features.

Emphasis is often put on the role of space discretization in energy budget consistency (Dukowicz and Smith, 1994; Adcroft et al., 1997; Roullet and Madec, 2000; Griffies et al., 2001) but rarely on time stepping effects. Despite this, very few numerical simulations actually exhibit accurate energy conservation. The simple barotropic adjustment test presented here indicates that time stepping effects can be much larger than discretization in space. Therefore, we suggest that any energy conservation analysis should consider both the time and space discretization.

Backward time stepping is commonly used for the free surface equation (Dukowicz and Smith, 1994; Wolff et al., 1997; Marshall et al., 1997b) and results in energy loss (e.g., the simple barotropic adjustment test, Section 5.3). This requires some comments:

- (a) There is no doubt that the test (5.c) presented here is over simplified. The magnitude of energy loss is probably extreme, but is indicative of behavior in more realistic ocean models that use the same free-surface time stepping. Note that other time stepping methods such as the split explicit FS also damp the energy of the external mode since time averaging is used with the methods and is not supposed to be energy conserving.
- (b) According to Arakawa (1966)—and often quoted—energy conservation offers a limited advantage, mainly in terms of stability of the momentum advection discretization. To accurately represent the evolution of the distribution of energy as a function of scale, conservation of both energy and enstrophy are required. However, such a scheme (Arakawa, 1966) has not yet been successfully implemented in a z -coordinate OGCM, probably because it is not easily done. Regarding the stability objective, alternative methods exist to ensure a stable discretization of the momentum advection terms (see for e.g., Tartinville et al., 1998), as for instance energy decreasing schemes known as Total Variance Diminishing schemes.
- (c) In coarse resolution, non-eddy resolving models, the KE that the model contains is not representative of the real ocean KE which is mainly contained in the eddy field (Stammer and Böning, 1985). In this case energy conservation is perhaps not a major concern. However, when eddy motions are permitted, low energy dissipation numerics are required in order to carry out accurate simulations of ocean dynamics. For this purpose, a relatively accurate energy conservation is sufficient and does not need to be exact. This justifies some recent developments which are presented as energy conserving (Adcroft et al., 1997; Roullet and Madec, 2000; Griffies et al., 2001), even if conservation is not exact because of the free-surface time stepping.

Depending on the particular application, the damping of the fast external gravity waves can be justified, providing it does not alter the essential features of interest. This is what happens when the backward time stepping and more generally a non-energy conserving free-surface method is used. In other applications, such as in the simple barotropic adjustment problem, an energy conserving scheme for the external mode, such as the Crank–Nickelson time stepping, is crucial.

The NLFS implementation in the MITgcm uses the implicit free surface method and allows us to select the external mode time stepping appropriate for each modeling study.

Acknowledgements

We wish to thank Stephen Griffies and an anonymous reviewer for constructive comments that greatly improved the manuscript. This work was supported by the ECCO project (Estimating the Circulation and Climate of the Ocean) and the MIT Climate Modeling Initiative.

Appendix A

The explicit integration of the column integrated continuity Eq. (4) was not present in the original model (Marshall et al., 1997a) and has been added for the purpose of the NLFS (see Section 2). However, for the linearized formulation, we find it useful to retain the integration of the linearized Eq. (4):

$$(h^{n+1} - h^n)/\Delta t = -\nabla \cdot H\mathbf{v}^n + P^n$$

in order to provide the SSH ($h^{n+1} - H$) on the right hand side of the linearized Eq. (10):

$$\eta^{n+1} - \beta\gamma\Delta t^2\nabla \cdot Hg\nabla\eta^{n+1} = (h^{n+1} - H) + \beta\Delta t P^{n+1} - \beta\Delta t\nabla \cdot H\mathbf{v}^* \quad (\text{A.1})$$

This is slightly different from the original, backward ($\beta = \gamma = 1$), linear free-surface formulation where η^n was used in place of $(h^{n+1} - H)$ in (A.1). The advantage of keeping an explicit integration of the continuity Eq. (4) is that it ensures an exact volume conservation (see 5.a for a quantitative estimation).

References

- Adcroft, A., Campin, J.-M., Heimbach, P., Hill, C., Marshall, J., 2002. MITgcm release 1 manual. Technical report, Massachusetts Institute of Technology, Cambridge, MA, 346 pp. <http://mitgcm.org/sealion>.
- Adcroft, A., Hill, C., Marshall, J., 1997. Representation of topography by shaved cells in a height coordinate ocean model. *Monthly Weather Review* 125, 2293–2315.
- Arakawa, A., 1966. Computational design for long-term numerical integration of the equations of fluid motion: Two-dimensional incompressible flow. Part I. *Journal of Computational Physics* 1, 119–143.
- Dukowicz, J.K., Smith, R.D., 1994. Implicit free-surface method for the Bryan-Cox-Semtner ocean model. *Journal of Geophysical Research* 99, 7991–8014.
- Griffies, S., Böning, C., Bryan, F., Chassignet, E., Gerdes, R., Hasumi, H., Hirst, A., Treguier, A.-M., Webb, D., 2000. Developments in ocean climate modelling. *Ocean Modelling* 2, 123–192.
- Griffies, S., Pacanowski, R., Schmidt, M., Balaji, V., 2001. Tracer conservation with an explicit free surface method for z-coordinate ocean models. *Monthly Weather Review* 129, 1081–1098.
- Huang, R.X., 1993. Real freshwater flux as a natural boundary condition for the salinity balance and thermohaline circulation forced by evaporation and precipitation. *Journal of Physical Oceanography* 23, 2428–2446.
- Killworth, P.D., Stainforth, D., Webb, D.J., Paterson, S.M., 1991. The development of a free surface Bryan-Cox-Semtner model. *Journal of Physical Oceanography* 21, 1333–1348.
- Marshall, J., Adcroft, A., Hill, C., Perelman, L., Heisey, C., 1997a. A finite-volume, incompressible Navier Stokes model for studies of the ocean on parallel computers. *Journal of Geophysical Research* 102, 5753–5766.

- Marshall, J., Hill, C., Perelman, L., Adcroft, A., 1997b. Hydrostatic, quasi-hydrostatic, and nonhydrostatic ocean modeling. *Journal of Geophysical Research* 102, 5733–5752.
- Panchev, S., 1985. *Dynamic Meteorology*. Kluwer Academic, Dordrecht, Holland, p. 360.
- Roullet, G., Madec, G., 2000. Salt conservation, free surface, and varying levels: a new formulation for ocean general circulation models. *Journal of Geophysical Research* 105, 23927–23942.
- Stammer, D., Böning, C.W., 1985. Generation and distribution of mesoscale eddies in the North Atlantic Ocean. In: Krauss, W. (Ed.), *The Warmwatersphere of the North Atlantic Ocean*. Gedrüder Borntraeger, Berlin, Germany, pp. 159–193.
- Stommel, H., 1948. The western intensification of wind-driven ocean currents. *Transactions of the American Geophysical Union* 29, 206.
- Tartinville, B., Deleersnijder, E., Lazure, P., Proctor, R., Ruddick, K.G., Uittenbogaard, R.E., 1998. A coastal ocean model intercomparison study for a three-dimensional idealised test case. *Applied Mathematical Modelling* 22, 165–182.
- Wolff, J.O., Maier-Reimer, E., Legutke, S., 1997. The Hamburg Ocean Primitive Equation model HOPE. Technical Report 13, Max-Planck-Institut für Meteorologie, DKRZ, Hamburg, Germany, 98 pp.